Outflow Driven Turbulence in Molecular Clouds

Jonathan J. Carroll[1], Adam Frank[1], Eric G. Blackman[1], Andrew J. Cunningham[1,2]

johannjc@pas.rochester.edu

ABSTRACT

Feedback from protostellar outflows can strongly influence the nature of turbulence in regions of star formation. In our previous work Carroll et al. (2009) we demonstrated that outflows were able to drive supersonic turbulence at levels consistent with the scaling relations from Matzner (2007) although with a steeper velocity power spectrum than expected for a supersonic turbulent cascade. Here we perform higher resolution simulations that build upon our earlier results as well as simulations of turbulence driven by outflows within an environment subject to external forcing. We find that the presence of outflows within an externally driven turbulent environment produces a knee in the velocity power spectrum at the outflow scale and a steeper slope at sub-outflow scales than expected for a cascade model. We also find that the presence of outflows flattens the density spectrum at large scales effectively reducing the formation of large scale turbulent density structures. We also performed a resolution study and found that the steepness of the velocity power spectrum is quite insensitive to the numerical resolution implying the lack of a bottleneck in the turbulent cascade associated with numerical dissipation. Finally, we performed MHD simulations of outflows within an initially uniform magnetic field and found the outflows were inefficient at amplifying the magnetic field.

Subject headings: protostellar outflows, turbulence, star formation rate

1. Introduction

As in our previous paper Carroll et al. (2009) we consider a cloud of mean density ρ_0, with outflows occurring at a rate per volume $\mathcal{S}$ with momentum $\mathcal{P}$. This then defines

[1]Department of Physics and Astronomy, University of Rochester, Rochester, NY 14620

[2]Lawrence Livermore National Laboratory, Livermore, CA 94550

characteristic outflow scales of mass, length, and time (Matzner 2007)

$$\mathcal{M} = \frac{\rho_0^{4/7}\mathcal{P}^{3/7}}{\mathcal{S}^{3/7}} \quad \mathcal{L} = \frac{\mathcal{P}^{1/7}}{\rho_0^{1/7}\mathcal{S}^{1/7}} \quad \mathcal{T} = \frac{\rho_0^{3/7}}{\mathcal{P}^{3/7}\mathcal{S}^{4/7}}$$

Combining these gives other characteristic quantities. Of particular interest is the characteristic velocity and the characteristic wave number:

$$\mathcal{V} = \frac{\mathcal{L}}{\mathcal{T}} \quad \mathcal{K} = \frac{2\pi}{\mathcal{L}}$$

In our previous paper, we demonstrated that typical values for ρ_0, $\mathcal{P}$, and $\mathcal{S}$ given in Table 1 could drive supersonic turbulence consistent with these scaling relations. We also found evidence of a driving scale in the velocity spectrum at $\sim \mathcal{K}$ as well as a steeper velocity power spectrum at sub-outflow scales compared to results from simulations of supersonic turbulent cascades. Clumps in star forming regions will likely form within turbulent environments and star formation will occur in the presence of both outflow feedback as well as a turbulent cascade from the largest scales. Here we extend our previous study by considering the combined influence of external driving and outflow feedback with higher resolution simulations and by looking at the effect played by an initial uniform magnetic field.

2. Numerical Model

As in Carroll et al. (2009) we used an MHD code called AstroCUB. The code is 2nd order accurate in space and time and uses a non-split CTU method with upwinded CT as described by Gardiner & Stone (2008). All four of the simulations were performed on a periodic cube of length 1.48 pc $= 4\mathcal{L}$. Turbulence was driven into an initially uniform medium of density $\rho_0 = 2.51 \times 10^{-20}$ and mean particle weight of 2.1 amu at 10 K giving a sound speed of .20 km/s. The turbulence in each simulation was driven by some combination of outflow feedback (§2.1) and/or isotropic forcing (§2.2) described below. Many of the simulations used a coarser grid initially and then refined by a factor of two after an outflow time scale ($\mathcal{T}$) until the desired final resolution was reached. All of the spectra here were taken after at least one crossing time after refining. Table 2 gives an overview of the simulation setups and when each simulation was refined.

2.1. Outflow Feedback

During the runs with outflow feedback, highly collimated bipolar outflows of momentum $\mathcal{P} = 20.0 M_\odot$ km/s were launched at the volumetric rate of $\mathcal{S} = 58.4\mathrm{pc}^{-3}\mathrm{Myr}^{-1}$ or with a

Table 1. Outflow Scales

	cgs units	astronomical units
ρ_0	2.51×10^{-20} g cm^{-3}	371 M$_\odot$ pc^{-3}
$\mathcal{P}$	3.98×10^{39} g cm s^{-1}	20.0 M$_\odot$ km/s
$\mathcal{S}$	6.31×10^{-68} cm^{-3} s^{-1}	58.4pc^{-3} Myr^{-1}
$\mathcal{L}$	1.14×10^{18} cm	.370 pc
$\mathcal{T}$	1.07×10^{13} s	.338 Myr
$\mathcal{V}$	1.07×10^{5} cm/s	1.07 km/s

Table 2. Table of Runs

Run	β	Isotropic Forcing	Outflow Forcing	Regrid Time in $\mathcal{T}$ 64	128	256	512
HDI	···	Yes	No	···	···	···	0
HDOI	···	Yes	Yes	0	3	5	6
HDO	···	Yes	No	···	0	5	6
MHDO	.5	No	Yes	···	···	0	···

period of $T_{launch} = \mathcal{S}L^3 = 5.28$ kyr from cylindrical source regions randomly located and oriented with radius r_o. Instead of constantly setting the values of density and momentum within each launch region as in Carroll et al. (2009), constant source terms were calculated to supply the mass and momentum needed to maintain a constant density ρ_0 and axial velocity profile:

$$v_z = \begin{cases} 0 & : 0 \leq |z| < z_i \\ \text{sign}\,(z)\,\frac{V_o(|z|-z_i)}{\Delta z} & : z_i \leq |z| \leq z_i + \Delta z \end{cases}$$

The source terms for density S_ρ and momentum $S_{\rho\mathbf{v}}$ were calculated by substituting the launch profiles into the conservation equations and solving for a steady state solution.

$$\frac{\partial \rho}{\partial t} = -\nabla \cdot (\rho \mathbf{v}) + S_\rho = 0 \Rightarrow S_\rho = \nabla \cdot (\rho \mathbf{v}) \tag{1}$$

$$\frac{\partial \rho \mathbf{v}}{\partial t} = -\nabla \cdot (\mathbf{v} : (\rho \mathbf{v})) - \nabla P + S_{\rho \mathbf{v}} = 0 \Rightarrow S_{\rho \mathbf{v}} = \nabla \cdot (\mathbf{v} \colon (\rho \mathbf{v})) + \nabla P \tag{2}$$

The mass loss rate of each outflow was $\dot{M} = 2\pi r_o^2 \rho_0 V_o = 1.30 \times 10^{-4} M_\odot$/yr and the momentum injection rate was $\dot{\mathcal{P}} = \dot{M} V_o =$ giving a desired outflow duration of $t_o = \frac{\mathcal{P}}{\dot{\mathcal{P}}} = 2.34$ kyr. The actual duration of the outflow was modified slightly to allow for an exponential ramp down of the velocity while keeping the total momentum injected equal to $\mathcal{P}$. As well as injecting momentum, each outflow injected a total mass of $\dot{M} t_o = \frac{\mathcal{P}}{V_o} = .305 M_\odot$. The outflows injected more mass then would be expected for a $.5 M_\odot$ star ejecting 1/6 of its mass, but the high ratio of outflow velocity to turbulent velocity $\frac{V_o}{\mathcal{V}} = 61.2$ already makes the computation difficult and decreasing the mass ejected would only increase this difficulty. We therefore chose V_o so that the total change in mass over the course of an outflow time was less than 2%. Table 3 summarizes the outflow parameters.

2.2. Isotropic Forcing

In addition to forcing via outflow feedback, a constant isotropic solenoidal forcing function was used to mimic large scale driving. The mean acceleration of the isotropic forcing was $\langle \mathbf{a} \rangle = .95 \frac{\mathcal{V}}{\mathcal{T}}$ while the components and phases of each wavevector were chosen randomly. Table 4 lists the forcing vectors and phases for each wave mode. The total force applied to each cell is given by

$$\vec{a}\,(\vec{x}) = \sum_n \vec{A_n} \cos\left(\vec{k_n} \cdot \vec{x} + \phi_n\right) \tag{3}$$

Table 3. Outflow Params

description	symbol	value	comment
density	ρ_0	2.5×10^{-20} g/cm^3	$\cdots$
velocity	V_o	65.5 km/s	$\cdots$
duration	t_o	2.34 kyr	$\cdots$
period	T_o	5.28 kyr	$\cdots$
radius	r_o	5960 AU	$10\Delta x$ at 512^3
inner buffer	z_i	$2\Delta x$	1190 AU at 512^3
launch thickness	Δz	3580 AU	$6\Delta x$ at 512^3
opening angle	θ_o	0 °	$\cdots$
mass loss rate	$\dot{M}$	$1.30 \times 10^{-4} M_\odot$ yr^{-1}	$\cdots$

Table 4. Isotropic forcing components

$\vec{k}$	$\vec{A}$	ϕ
$[1, 0, 0]$	$[0, .04087, .81547]$	1.6519
$[0, 1, 0]$	$[-.64450, 0, -.50128]$	1.1919
$[0, 0, 1]$	$[-.41577, .70271, 0]$	3.7784

3. Results

3.1. Outflow feedback within a turbulent cascade

Figure 1 shows the typical growth and saturation of various quantities for Run II. Initially the mean scalar momentum density $P_{mag} = \langle \rho |v| \rangle$ is accelerated by outflows and the isotropic forcing both at a rate $\frac{\rho_0 \mathcal{V}}{\mathcal{T}}$ giving a net forcing $\frac{dP_{mag}}{dt} = 2\frac{\rho \mathcal{V}}{\mathcal{T}}$. At $\sim 2\mathcal{T}$ the dissipation of momentum becomes comparable to the injection of momentum and the turbulence saturates. At $8\mathcal{T}$ the outflows are turned off but the isotropic forcing is left the same (Run IIb). There is an apparent oscillating component to v_{rms} with a period equal to $4\mathcal{T}$ associated with the external forcing: $\tau_{ex} = \frac{L_{box}}{v_{ex}} = \frac{4\mathcal{L}}{\mathcal{V}} = 4\mathcal{T}$. The plot of the energy weighted density, shows that the bulk of the energy is in low density flows associated with the expanding cavities. This low density high velocity component is also apparent in figure 2. Both Run II and Run IIb show lognormal distributions of density however Run II shows a much broader range in both velocity and density then Run IIb.

Figure 3 shows the velocity and density power spectrum for runs I, II, and IIb. As in Carroll et al. (2009) the presence of outflows tends to increase the slope of the velocity spectrum at sub-outflow scales. We also find that the density spectrum at supra-outflow scales is quite flat when outflows are present even in the presence of isotropic forcing of comparable strength.

3.2. Resolution study

To better understand the role numerical dissipation might play in the density and velocity spectra, we completed Run II at $64^3, 128^3, 256^3$ as well as 512^3 in order to perform a resolution study. Figure 3.2 shows both velocity and density power spectra for run II at $\sim 8\mathcal{T}$ at resolutions of 64^3, 128^3, 256^3, and 512^3. The velocity spectra seem fairly insensitive to numerical resolution at sub-outflow scales, while the density spectra seem to flatten with higher resolution and turn downward at scales smaller then $8\Delta x$ where Δx is the grid spacing.

3.3. Magnetic Fields

We find that an initial uniform magnetic field is amplified by the outflows although the rate at which the outflows are able to amplify the fields is reduced after the initial round of outflows has compressed the magnetic field into high density filaments. We conclude that

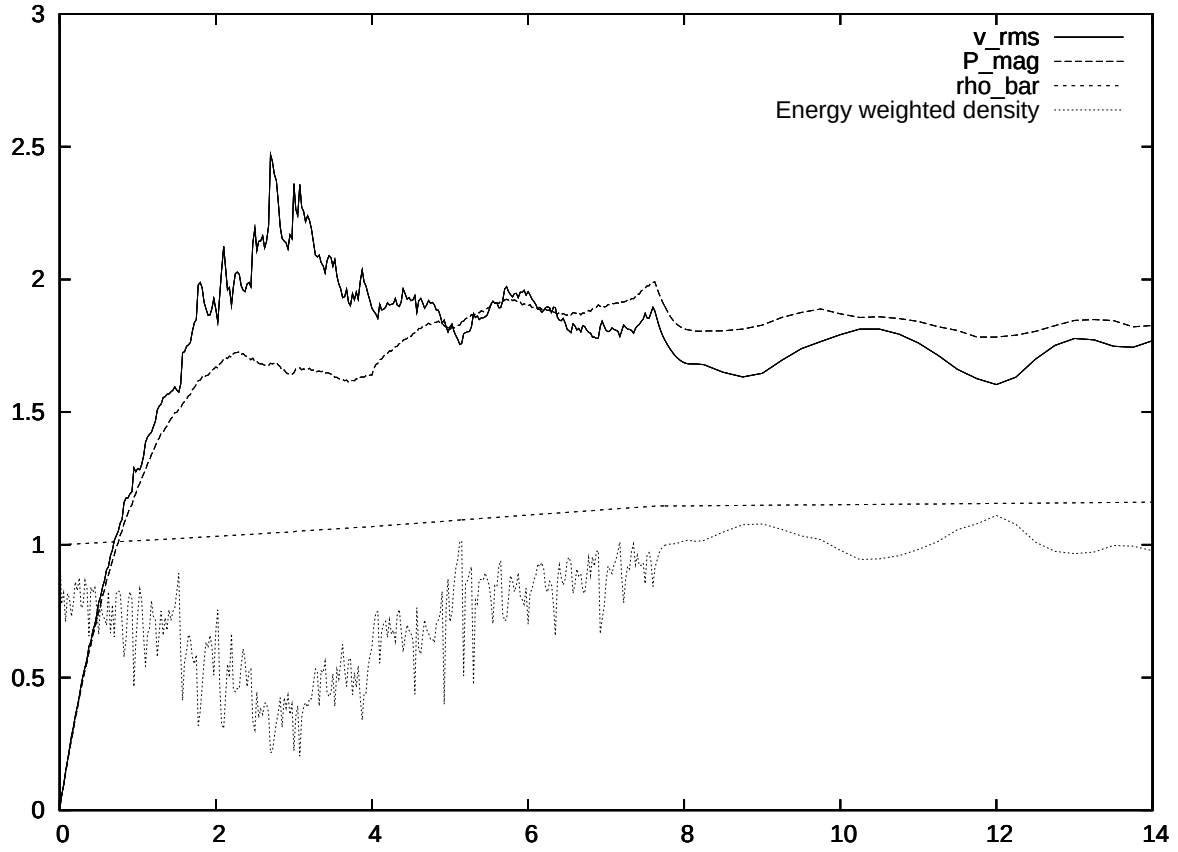

Fig. 1.— Time series showing development of the root mean squared velocity v_{rms}, total scalar momentum P_{mag}, average density $\bar{\rho}$, and specific kinetic energy weighted density $\rho_{v^2} = \frac{\langle \rho v^2 \rangle}{\langle v^2 \rangle}$

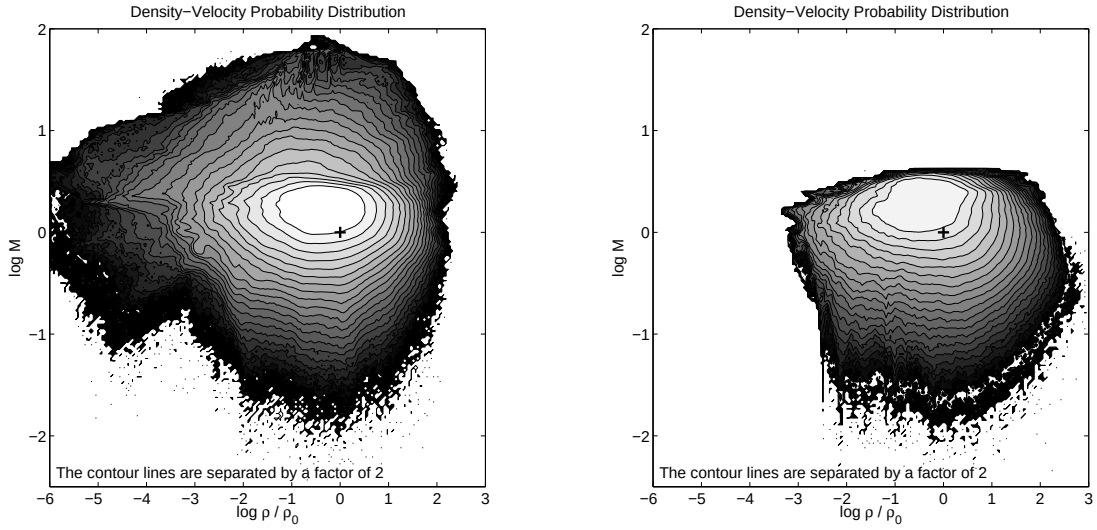

Fig. 2.— Joint probability distribution functions for turbulence by both outflows and external forcing (left), and with just external forcing(right)

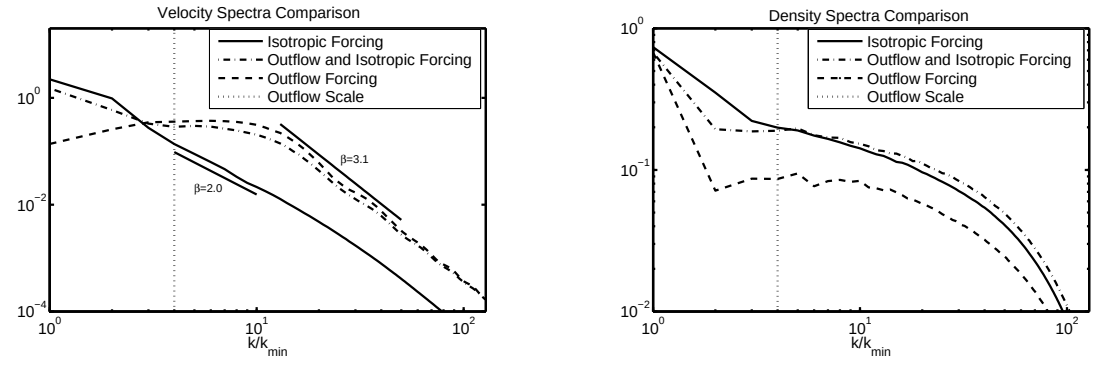

Fig. 3.— Velocity power spectrum (left) and density spectrum (right) for turbulence created by jets alone, isotropic forcing alone, and combined forcing.

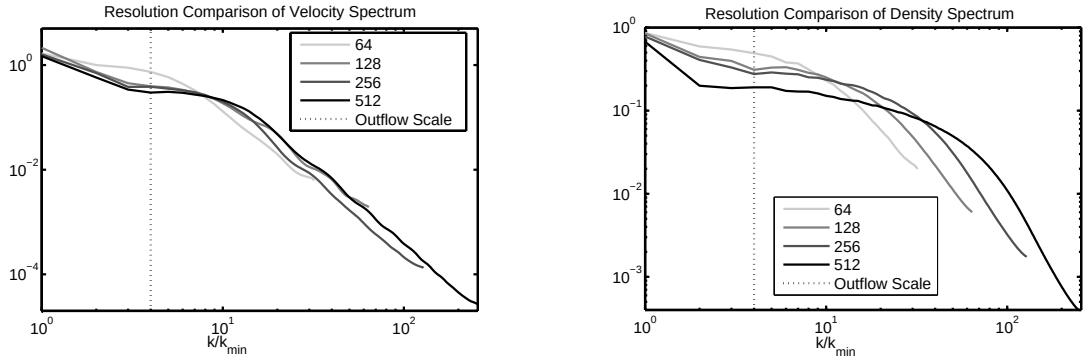

Fig. 4.— Plot showing velocity and density power spectrum at different resolutions. Note the insensitivity of the velocity spectrum to resolution at sub-outflow scales especially when compared to the density spectrum

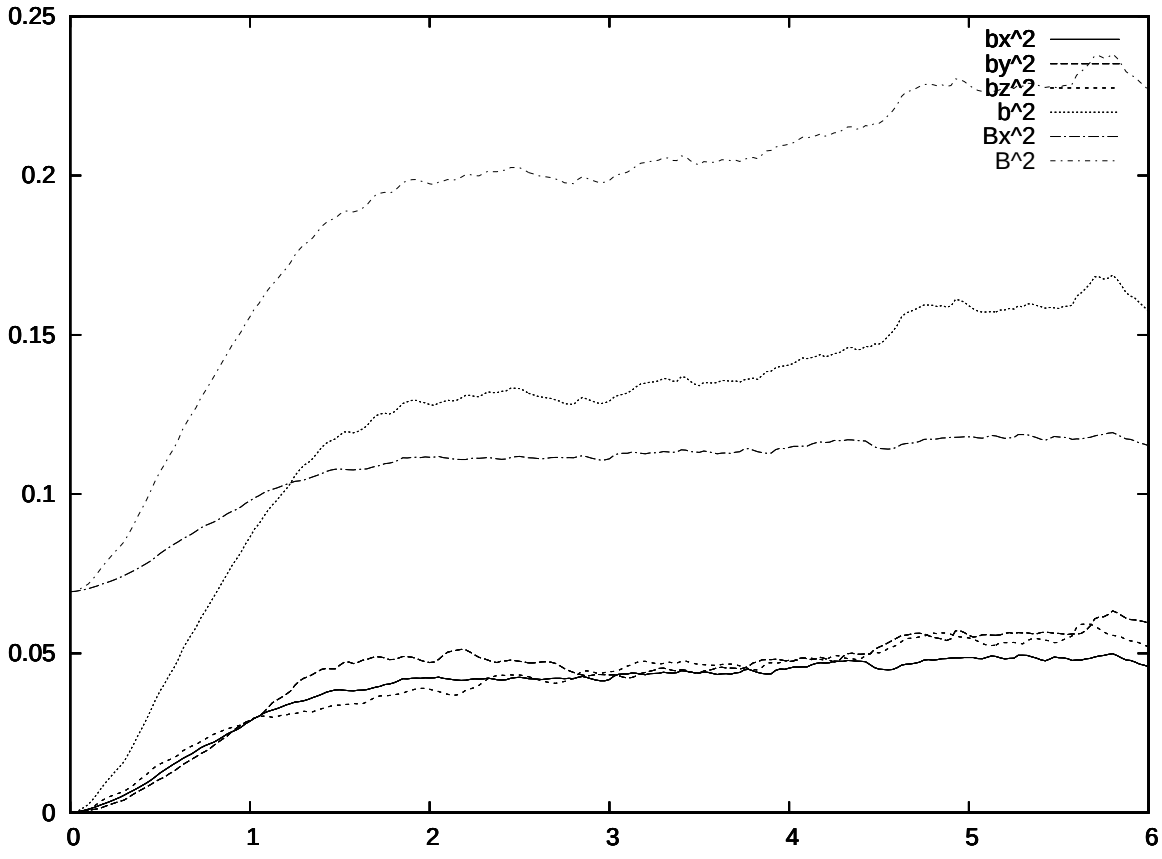

Fig. 5.— Plot showing time development of magnetic energy for run IV. Note the initial ambient thermal pressure is $\frac{c_s^2}{v^2} = .0347$

outflow feedback is not an efficient source of magnetic field amplification and that gravity or large scale shear would provide a better means for magnetic amplification.

4. Discussion

Building on the work of Carroll et al. (2009) we looked at the role numerical resolution played on the development and characteristics of outflow driven turbulence. We carried out simulations of turbulence driven by both external (isotropic) forcing and internal (outflow) forcing at resolutions of 64^3, 128^3, 256^3, and 512^3. We find that the conclusions of Carroll et al. (2009) hold at higher resolution and that the slope of the velocity spectrum is surprisingly insensitive to the numerical resolution. Were numerical dissipation primarily responsible for the steep velocity spectrum, we would expect to see evidence of a resolution dependent bottleneck effecting the shape and steepness of the velocity spectrum. The lack of any such bottleneck supports our previous conclusion that the steeper velocity spectrum is due to the nature of the outflow forcing. At large scales, the density spectra tends to flatten with increased resolution while at smaller scales it tends to steepen at a resolution dependent scale of $\sim 8\Delta x$ due most likely to the resolution dependent thickness of the isothermal shocks.

Comparisons between isotropically forced turbulence, outflow driven turbulence, and turbulence generated by both outflows and isotropic forcing show clearly the effect of outflow feedback. The outflows still produce a knee in the spectra at the outflow scale and a steeper fall off at sub-outflow scales indicating a suprising lack of an energy cascade to small scales. The lack of an energy cascade effectively reduces the efficiency with which outflow driven turbulence decays and ... ??? In addition to a steeper velocity spectra at sub-outflow scales, we find a flatter density spectra at supra-outflow scales then what is seen for a supersonic turbulent cascade (see figure 3). In the absence of outflows, large scale motions are able to create large scale density structures. Outflows however, continuously disrupt these large scale structures from forming on timescales $\sim \mathcal{T}$ and instead produce a whiter spectrum. See figure 4. Outflow feedback is therefore important in not only driving clump supporting turbulence, but also in limiting the spatial scales of density structures and therefore shaping the IMF (initial mass function). Wang et al. (2009) also found that by including self-gravity and self-consistently placing and orienting outflows, that the star formation rate (especially of massive stars) was significantly reduced by the outflow feedback.

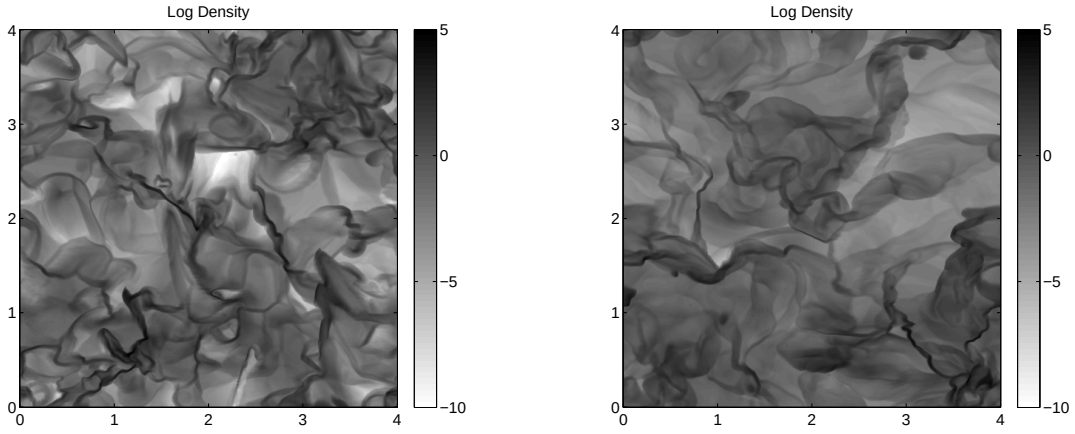

Fig. 6.— Plots showing log density for turbulence driven by outflows and isotropic forcing (left panel) and isotropic forcing only (right panel). All plots are scaled to ρ_0

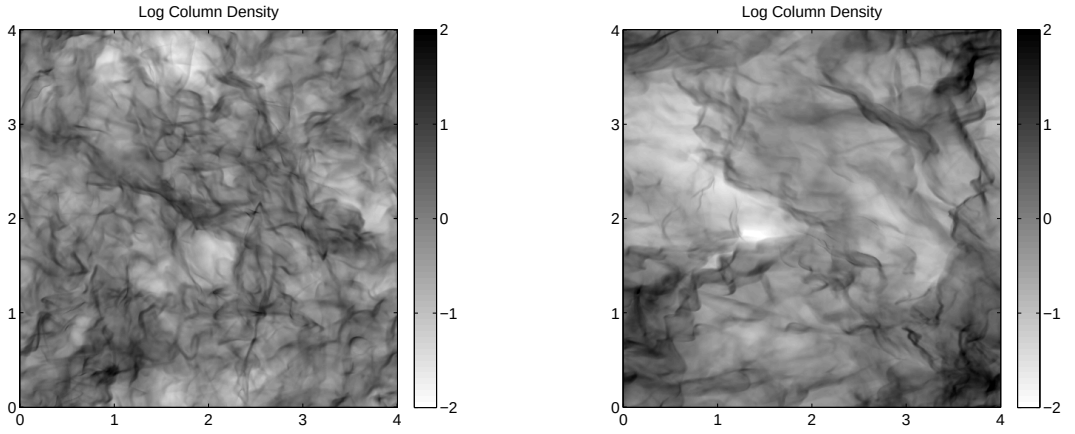

Fig. 7.— Plots showing log column density for turbulence driven by outflows and isotropic forcing (left panel) and isotropic forcing only (right panel). All plots are scaled to ρ_0

4.1. Principal Component Analysis

4.2. Velocity Centroid Analysis

Since most inferences of velocity spectra from observations are based on emission, and emission is stongly dependent on density, the flattened density spectra might mask the steeper velocity spectra. To this end we performed velocity centroid analysis on synthetic emission maps of an optically thin tracer where the emission was directly proportional to the density. Figure 4.2 shows the lack of a knee at the outflow scale and in fact shows no evidence of outflow driving at all.

5. Conclusion

Outflows drive and sustain supersonic turbulence. Outflows produce a knee in the turbulent spectrum. Outflow driven turbulence has a steeper velocity spectrum than cascade models. Outflow driven turbulence has a shallower density spectrum Outflows are able to enhance magnetic fields initially present, though not to equipartition with kinetic energy. Further comparisons between simulation and observation are needed to understand the role of feedback and star formation.

REFERENCES

Carroll, J., Frank, A., Blackman, E. G., Cunningham, A. J., & Quillen, A. C. 2009, apj, 695, 1376

Gardiner, T. A. & Stone, J. M. 2005, JCP 205, 509

Table 5. Autocorrelation lengths of eigenimages from principal component analysis

Run	l_1	l_2	l_3	$\frac{l_2}{l_1}$
HDI	.4204	.1440	.1066	
HDOI	.4699	.1680	.0663	.3574
HDO	.4957	.0470	.0286	.09480

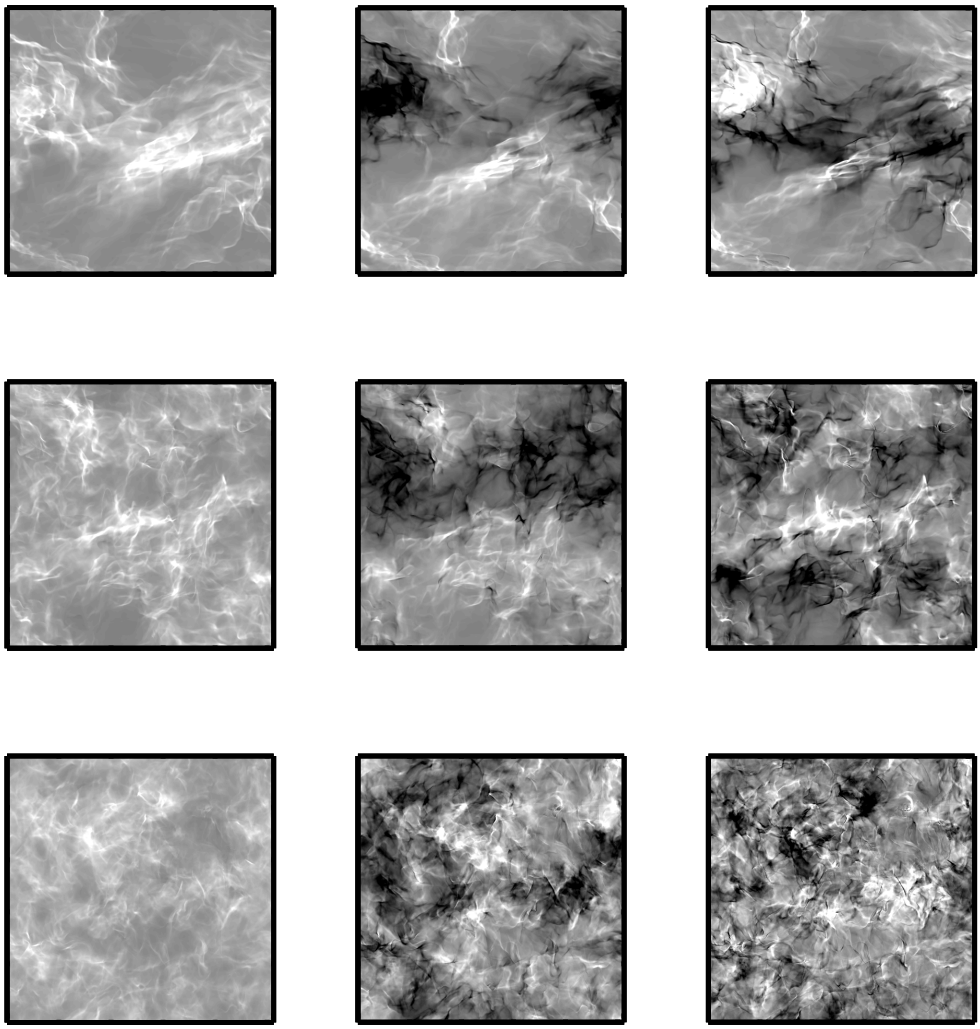

Fig. 8.— Plot showing power spectrum of velocity centroids along line of sight

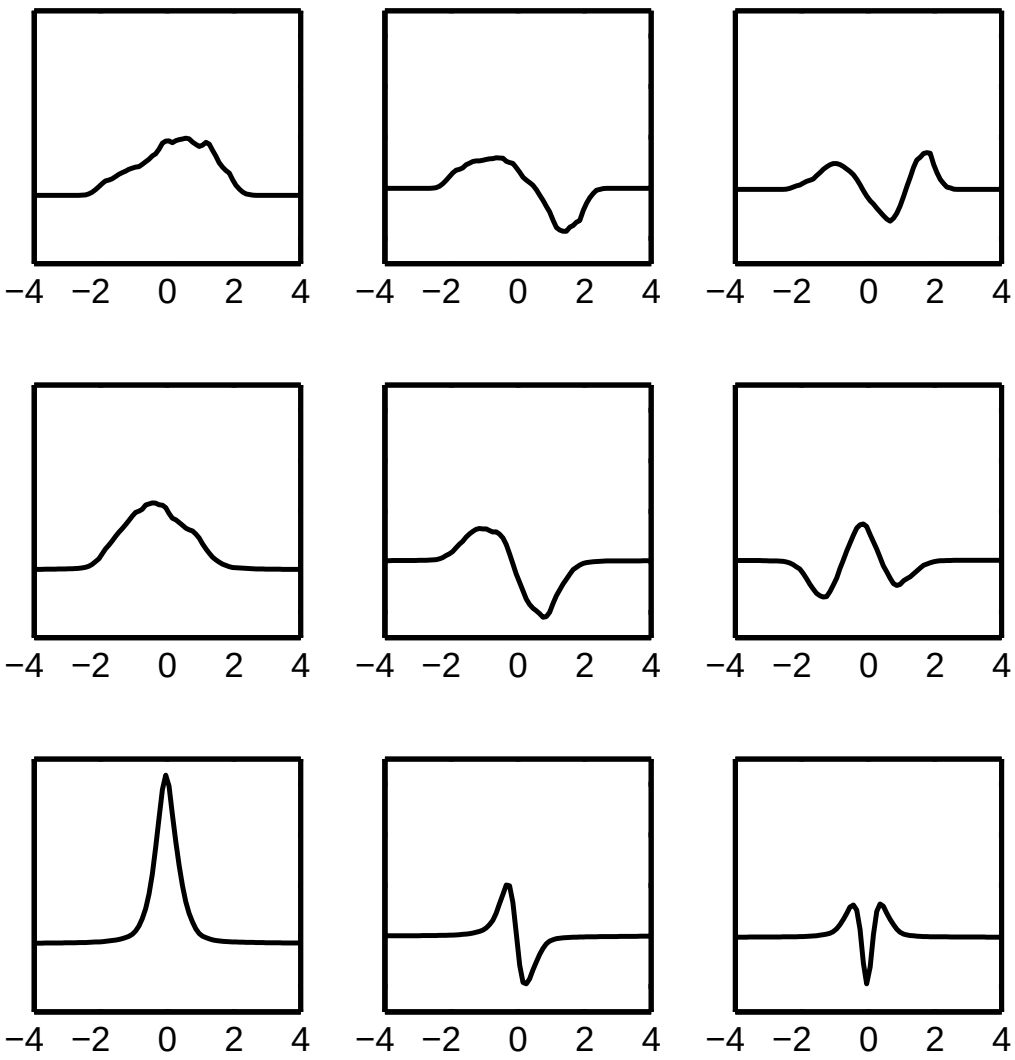

Fig. 9.— Plot showing power spectrum of velocity centroids along line of sight

Gardiner, T. A. & Stone, J. M. 2008, JCoPh 227, 4123

Matzner, C. D. 2007, ApJ, 659, 1394

Wang, P., Li, Z. Y., Abel, T., & Nakamura, F. 2009, ArXiv e-prints, 908, arXiv0908.4129W